PHYSICS OF FLUIDS **28**, 083302 (2016)

Microscopic origin of self-similarity in granular blast waves

M. Barbier,[1] D. Villamaina,[2] and E. Trizac[3]
[1]*Department of Ecology and Evolutionary Biology, Princeton University, Princeton, New Jersey 08544, USA*
[2]*Laboratoire de Physique Théorique de l'ENS (CNRS UMR 8549) and Institut de Physique Théorique Philippe Meyer, 24 Rue Lhomond, 75005 Paris, France*
[3]*LPTMS, CNRS, Univ. Paris-Sud, Université Paris-Saclay, 91405 Orsay, France*

(Received 7 June 2016; accepted 3 August 2016; published online 16 August 2016)

The self-similar expansion of a blast wave, well-studied in air, has peculiar counterparts in dense and dissipative media such as granular gases. Recent results have shown that, while the traditional Taylor-von Neumann-Sedov (TvNS) derivation is not applicable to such granular blasts, they can nevertheless be well understood via a combination of microscopic and hydrodynamic insights. In this article, we provide a detailed analysis of these methods associating molecular dynamics simulations and continuum equations, which successfully predict hydrodynamic profiles, scaling properties, and the instability of the self-similar solution. We also present new results for the energy conserving case, including the particle-level analysis of the classic TvNS solution and its breakdown at higher densities. *Published by AIP Publishing.* [http://dx.doi.org/10.1063/1.4961047]

I. INTRODUCTION

A blast is a shock wave that follows the sudden release of a large amount of energy in a small volume of gas — typically due the detonation of an explosive. The volume of gas is heated to large temperatures, thus large pressures, and starts expanding, causing a decrease of density at the center and a corresponding increase toward the boundaries. In the case of "strong shocks," the displaced matter moves faster than energy can be transported into the environment by sound or heat waves, and there is thus a discontinuity between a well-defined expanding perturbed zone and the surrounding gas, still at rest. This compression shock front is characterized by a sharp gradient in density and other hydrodynamic fields.

In air and similar conservative gases, it is well known that, as long as this strong shock condition is verified, the expansion of the bulk of the blast is self-similar in time: it exhibits a fixed internal structure, which simply scales up over the course of the dynamics. Furthermore, all the scaling laws for observables are easily derived from dimensional analysis. This in turns allows for greatly simplified, even solvable, theoretical descriptions,[1,2] and has been studied experimentally in a number of systems, from air[3] to laser-induced shocks in plasmas[4,5] or astrophysical systems such as supernova remnants[6] (the interaction of ejecta from stellar explosions with the surrounding environment).

Many applications however diverge from the prototypical example of air, by involving media that dissipate energy or momentum due to radiation, inelastic collisions, or drag.[7,8] They may also exhibit high or inhomogeneous density and other specific features, from chemical reactions (e.g., flame fronts) to bubble formation[9] and damping in underwater explosions.[10,11] In many cases, self-similar expansion can still be observed, although scaling properties can generally no longer be explained by mere dimensional analysis. A striking counter-example to the latter is the asymptotic scaling regime of the blast in an energy-dissipating medium such as radiative plasma or granular gas. Contrary to one common use of the word "dissipative" in hydrodynamics, we do not simply mean that flow energy is dissipated into random agitation, but that energy is lost from the system altogether, e.g., into microscopic degrees of freedom of the grains, or as radiation that leaves the fluid. As seen in Fig. 1, a blast wave in this setting takes a peculiar hollow shell structure, whose expansion can be entirely understood in terms of inertial motion.

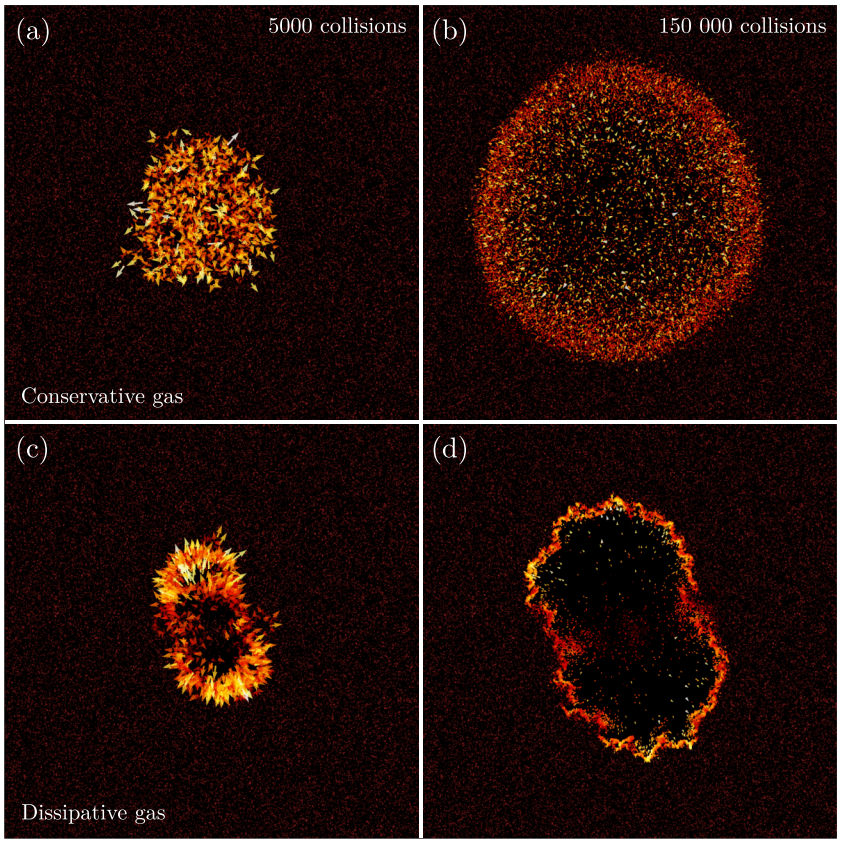

FIG. 1. Snapshots of a self-similar blast in molecular dynamics simulations, with particles indicated by disks and their velocities by arrows. The figure shows the collision cascade after 5×10^3 (left) and 1.5×10^5 (right) collisions, starting with two particles at the center with equal and opposite initial velocities. (a) and (b) Conservative blast. (c) and (d) Dissipative blast. The two differ in a number of ways; most strikingly, the conservative blast restores its rotational symmetry while anisotropy is preserved by dissipative dynamics, which also lead to a hollow core devoid of particles.

Across this wide range of problems, approaches can broadly be divided into three categories, depending on the level of description that they adopt:

- Scaling laws for macroscopic quantities such as the radius $R(t)$ and the energy $E(t)$, derived from considerations on conservation laws and fluxes at the boundaries.[7]
- Continuum media descriptions: hydrodynamic models and finite-element (or analogous) simulations.[12,13]
- Particle-level descriptions: kinetic theories and molecular dynamics simulations.[14]

A thorough understanding of self-similarity may often require the joint use of all three types of approaches. For the dissipative blast in particular, it has long been suggested that the global invariant driving this similarity regime is conserved radial momentum;[15] however, a microscopic justification for how this regime comes about and is maintained has been lacking, and the previous attempt at a continuum description has not been empirically validated.[8] Unfortunately, the latter two types of approaches, coarse-grained and microscopic, have so far remained largely impervious to each other.

Following the success of Taylor[2] and others, blasts have long been associated with continuum descriptions, which comprise the vast majority of the literature on this topic.[6,7,16] However, some of the assumptions underlying these analyses, and even the associated simulations, are questionable in the absence of microscopic scrutiny. Indeed, the derivation of hydrodynamic equations, and constitutive relations for pressure and transport terms, assumes local thermodynamic equilibrium conditions at each point of the medium. This can fail in shockwaves,[17] especially within the shock front, traditionally considered as a singular boundary in continuum equations, where hydrodynamic

fields undergo large changes over very small distances. These assumptions are also problematic in non-conservative fluids. Few continuum descriptions are rigorously derived from microscopic dynamics, and they are rarely, if ever, connected to the existing body of knowledge on blasts.

On the other hand, particle-level approaches have only recently turned to the question of blast waves.[14] This initiative mostly stems from the study of granular gases, which has opened a new arena in shock wave dynamics:[18] these fluids of macroscopic grains provide a direct window into kinetic phenomena, and have been offered as a prototype for understanding energy-dissipating media.[19] As we will show, this is especially true in the case of the dissipative blast: under weak conditions, its self-similar growth does not depend on the specifics of the dissipation mechanism, and one can confidently use a granular gas as a model system for other dissipative fluids, allowing for a detailed grasp of phenomena that may also occur in laboratory plasmas and astrophysical systems. Blast experiments in granular fluids[20,21] and particle based simulations[22] have been performed in recent years, giving snapshots such as those in Fig. 1 of the peculiar structure of the shock. They have now been successfully analyzed by a continuum description.[23] This multilevel approach is explained in detail here, and applied back to the original problem of conservative fluids, leading to the first molecular dynamics validation of the Taylor model, its extension to a more general constitutive relation, and the discovery of its breakdown at higher densities. This approach calls for replication for other self-similar phenomena driven by global invariants, which may likewise find relevance beyond granular systems.

The plan of this article is as follows. In Sec. II, we expound on the hydrodynamic framework: first, for a conservative blast according to the Taylor-von Neumann-Sedov (TvNS) approach, which we generalize to higher densities and confront to simulation results; then, in the presence of dissipation, which requires a new approach based on a multi-layered structure. From there, we explain the peculiar scaling of the radius $R(t)$ of the dissipative blast in Sec. III. Finally, we describe in Sec. IV the mechanisms through which the previously derived hydrodynamic solution becomes asymptotically unstable, and we explain the self-similar growth of this corrugation instability. In the supplementary material, we provide a more detailed introduction to previous results on blast waves, their self-similarity properties, and the study of shock waves in the granular fluid literature. We also give more extensive information on mathematical and numerical methods. Preliminary accounts of parts of this work were published in a short communication.[23]

II. HYDRODYNAMICS

A. Framework

Previous approaches of the dissipative blast have been rooted in the study of astrophysical or laboratory plasmas, and thus rely on hydrodynamic descriptions for these fluids. As clarified in the supplementary material, this description is much simplified by the self-similarity of the blast expansion: in an isotropic blast with central symmetry, all hydrodynamics fields depend on position $\mathbf{r}$ and time t only through the dimensionless variable $\lambda = r/R(t)$ with $r = |\mathbf{r}|$ and $R(t)$ the growing blast radius.

The study of granular gases lends itself naturally to a kinetic approach and molecular dynamics simulations. It is however possible to connect those to a hydrodynamic framework, by coarse-graining the particle-level description so as to define their number density $n(\mathbf{r},t)$ (locally averaged over realizations or with an appropriate smoothing kernel) as well as the mean $\mathbf{u}(\mathbf{r},t)$ and variance $\Theta(\mathbf{r},t)$ of their local velocity distribution. Number density n relates to mass density ρ through $\rho = mn$, with mass m hereafter fixed to unity. Equations thus obtained from kinetic theories and coarse-graining have the structure of hydrodynamic models, with coefficients expressed in terms of particle properties; they were first derived in the limit of dilute systems,[24,25] then extended to dense fluids of inelastic hard spheres.[26]

An important simplification in our case is that, since we are interested in a self-similar solution with growing length scale $R(t)$, spatial gradients tend to decrease in magnitude as for any field Ψ,

$$\frac{d}{dr}\Psi\left(\frac{r}{R(t)}\right) = \frac{1}{R(t)}\frac{d}{d\lambda}\Psi(\lambda). \tag{1}$$

Thus, terms of different order in spatial gradients will scale differently with $R(t)$ and decouple asymptotically. This property is especially interesting as the derivation of hydrodynamic equations from a kinetic framework involves an expansion in powers of the gradients, the Chapman-Enskog expansion,[27] which is only formal in most systems yet becomes exact in the bulk of the blast. More concretely, transport terms such as viscosity and heat conduction, involving higher-order gradients, cannot manifest at the same spatial scale as advection, i.e., $R(t)$; thus, we will see that the flow at that scale essentially obeys the Euler equations for a perfect fluid. The consequences of considering heat conduction have been discussed in the literature and shown to hold only for a limited time.[28]

Up to the first order in gradients, the equations for the local evolution of mass, momentum, and energy in the inelastic hard sphere framework[26] take the standard form of compressibility, Navier-Stokes and heat equations,[29]

$$\partial_t n + \nabla(n\mathbf{u}) = 0, \tag{2a}$$

$$(\partial_t + \mathbf{u}.\nabla)\mathbf{u} + \frac{1}{n}\nabla.\mathbf{p} = 0, \tag{2b}$$

$$n(\partial_t + \mathbf{u}.\nabla)\Theta + (\gamma - 1)(\mathbf{p}.\nabla)\mathbf{u} = -\Lambda, \tag{2c}$$

where the adiabatic index is given by $\gamma = 1 + \frac{2}{d}$ for hard spheres in spatial dimension d. The pressure tensor $\mathbf{p}$ must be further specified in terms of the fields by a constitutive relation, as discussed below. The only term specific to dissipative fluids is the energy sink Λ given by

$$\Lambda = \omega(1 - \alpha^2)n\Theta, \tag{3}$$

where $\omega = \omega_0(n\Theta)^{1/2}$ is the collision frequency in the gas, proportional to the average relative velocity and the inverse of the mean free path,[26,30] with ω_0 a dimensionless constant. The constant α is known as the restitution coefficient, and $(1 - \alpha^2)$ represents the average fraction of thermal energy lost in each collision: if $\alpha = 1$, collisions are elastic, and if $\alpha = 0$, they are maximally dissipative. It is known in granular systems that α for any collision may in fact be a function of the relative velocity of particles,[31] but here we will show that any $\alpha < 1$ will lead to the same asymptotics, and we can thus assume α to be constant without loss of generality.

A similar energy sink term occurs in the description of radiative plasmas, where it is expected to exhibit some power-law dependence in n and Θ,

$$\Lambda = \Lambda_0 n^{\mu+1}\Theta^{\nu+1}, \tag{4}$$

with Λ_0 an appropriate dimensional constant. The energy dissipation rate, having the dimensions of an inverse time, is thus given by $\Lambda_0 n^\mu \Theta^\nu$, where exponents μ and ν depend on the cooling mechanism: they encapsulate how both the frequency of dissipative events and the amount of energy dissipated in each event scale with density and temperature. When the origin of dissipation is collisional, as in granular flows or dust cooling in interstellar media[16] (the plasma losing energy through collisions between ions and dust particles), we expect $\mu > 0$ and $\nu > 0$ as collisions become more frequent with higher agitation and density. For dissipative hard spheres, $\mu = \nu = \frac{1}{2}$. Indeed, the r.h.s. of Eq. (3) can be rewritten as $\Lambda_0(\alpha)\,(n\Theta)^{3/2}$ where we identify $\Lambda_0(\alpha) = \omega_0(1 - \alpha^2)$. A very different behavior[32] can be expected to arise depending on the sign of μ and ν. However, if both are positive — as is the case here — we argue that the solution is largely independent of the specific values of these exponents: the same blast structure (described below) will be established for any $\mu, \nu > 0$, as the energy sink then exceeds the advection terms in Eq. (2c), and all temperature is dissipated within a comparatively thin cooling layer. The exponents μ and ν may control the precise features of that layer (including the scaling of its width), but they will not alter the scaling and stability properties of the blast, which we show below are all driven by the inner cold region where motion is strictly coherent.

B. Constitutive relation and boundary conditions

The hydrodynamic equations (2) are closed by specifying the pressure tensor $\mathbf{p}$ with a constitutive relation or equation of state. It may be assumed to have vanishing non-diagonal terms: they are associated with transport phenomena (i.e., viscosity) involving higher-order gradients.[33] As

argued above, those are irrelevant here because their scaling in the growing length scale $R(t)$ will generically differ from that of the terms in Eqs. (2), causing asymptotic decoupling.

In hydrodynamic models, the diagonal component of pressure is commonly assumed to be isotropic, i.e., $\mathbf{p} = p\mathbf{I}$ with $\mathbf{I}$ the identity tensor. This is a natural consequence of the existence of a local equilibrium at every point in the fluid, which underlies standard hydrodynamics. However, this assumption does not necessarily hold in granular systems, or dissipative fluids in general, and indeed will be challenged below. Instead, we propose that a solution can be found with

$$\mathbf{p} = p\,\mathbf{e}_p, \tag{5}$$

where $\mathbf{e}_p$ is a tensor reflecting the directionality of pressure and will be specified as needed. As for the scalar magnitude p, the dense transport framework for hard spheres[26] suggests the constitutive relation,

$$p = n\Theta Z(n), \tag{6}$$

where $Z(n)$ stems from the finite compressibility of the gas. In the dilute limit, $Z(n \to 0) \to 1$ and the relation above becomes the ideal gas law (note that k_B does not appear as Θ is an energy rather than a thermodynamic temperature). However, $Z(n)$ diverges at finite n to account for the increase of pressure due to steric effects. Numerous functional forms[34] have been proposed for $Z(n)$; for our two-dimensional study, we choose the classic Henderson relation[35]

$$Z(n) = \frac{1 + \varphi(n)^2/8}{(1 - \varphi(n))^2} \tag{7}$$

with the volume fraction $\varphi(n)$ occupied by the particles, as defined in the supplementary material. This relation is derived under equilibrium conditions; yet, it is found to provide good agreement between theoretical and numerical results, even as it is used here to describe the strongly out-of-equilibrium flow in the blast wave, and especially within the shock front. Other plausible candidates[36] were found to provide comparably good results.

This specification of the constitutive relation is an important step in our analysis, as we show below that even in the well-known conservative blast, numerical results at moderate densities can disagree significantly with the standard TvNS solution. This discrepancy is a new result and will also provide an occasion to recall steps of the standard method that prove useful for our discussion of the dissipative blast.

We must additionally remark that with a nontrivial constitutive relation $Z(n) \neq 1$, another term enters in the expression of the energy dissipation, which is now properly written as

$$\Lambda = \Lambda_0(\alpha)\,(n\Theta)^{3/2} - \Lambda_1(\alpha)\,(1 - Z^{-1}(n))(\mathbf{p}.\boldsymbol{\nabla}).\mathbf{u}. \tag{8}$$

The second term is seen to be structurally similar to one term from Eqs. (2). Indeed, while the last term in the l.h.s. of Eq. (2c) signifies the creation of random motion (kinetic temperature) by pressure along a velocity gradient, this term represents the energy dissipated in that process. It means that less agitation is generated in a dissipative fluid, and the two terms can be combined into one by using an effective adiabatic index $\gamma^*(n, \alpha)$. Various expressions[37,38] have been proposed for the prefactor $\Lambda_1(\alpha)$. While this new term should be included to achieve a consistent level of approximation throughout the equations, we found that it did not alter the results perceptibly, and ignored it for simplicity.

Once the hydrodynamic equations are closed by the choice of an appropriate equation of state, a solution for the fields is entirely specified by its boundary conditions. In our case, the natural boundary is the shock front: the layer separating the bulk of the blastwave from the external medium. It has a clear microscopic definition, as the region within which excited particles mix and collide with particles at rest, creating incoherent motion — "temperature." The radius of the blast $R(t)$ can thus be defined either as the inner limit of the shock front, so as to cover only excited particles, or as its outer limit, so as to exclude only particles at rest; we will opt for the former definition so that all particles within the blast are excited, which, for instance, allows this whole region to be self-similar in the TvNS solution.

Computing the boundary values of the fields can be done using the classic Rankine-Hugoniot conditions, and following the derivation detailed in the supplementary material, we find the relationships between the values on the inside (subscript 1) and on the outside (subscript 0) boundaries of the shock front,

$$\begin{aligned} n_1 &= \left(\frac{2}{(\gamma-1)\ Z(n_0)}+1\right) n_0, \\ u_1 &= \dot{R}\left(1-\frac{n_0}{n_1}\right), \\ P_1 &= n_0 \dot{R}^2 \left(1-\frac{n_0}{n_1}\right), \end{aligned} \tag{9}$$

where the last two relations are conveniently expressed in terms of (the inverse of) the compression ratio n_1/n_0.

C. Conservative blast and breakdown at high density

We start by specifying the conditions for the classic TvNS solution. In the particular elastic case ($\alpha = 1$, hence $\Lambda = 0$), and with the standard assumption of an isotropic pressure tensor $\mathbf{p} = p\mathbf{I}$ ($\mathbf{I}$ being the identity matrix), the Euler equations for a perfect fluid are recovered from Eqs. (2). Within the blast, a solution can be found with the ansatz that the fields adopt a scaling form: as argued in Appendix 1 of the supplementary material, the location of a point within the structure of the blast is indexed by a single dimensionless variable $\lambda = r/R(t)$ and we may rewrite the fields as follows:

$$\begin{aligned} n(\mathbf{r},t) &= n_0 M(\lambda), \quad \mathbf{u}(\mathbf{r},t) = \frac{\mathbf{r}}{t} V(\lambda), \\ \Theta(\mathbf{r},t) &= \frac{r^2}{t^2} T(\lambda), \quad p(\mathbf{r},t) = n_0 \frac{r^2}{t^2} P(\lambda), \end{aligned} \tag{10}$$

where the prefactor is the dimensionally appropriate combination of dimensional parameters r, t and the initial homogeneous number density n_0 (we recall that mass has been taken equal to unity). The choice of nondimensionalization will simply change the functional forms for M, V, T, and P, which are the dimensionless profiles that fully characterize the self-similar solution.

Let us further denote by δ the scaling exponent in $R(t) \sim t^\delta$, so that $\dot{R} = R\delta/t$. Equations (2) then become ordinary differential equations on the dimensionless profiles,

$$\begin{aligned} &M'(V-\delta) + M(dV + V') = 0, \\ &V'(V-\delta) + V(V-1) + \frac{2P+P'}{M} = 0, \\ &T'(V-\delta) + 2T(V-1) + (\gamma-1)\frac{P}{M}(dV+V') = 0, \end{aligned} \tag{11}$$

where we use the notation

$$\Psi' = \lambda \frac{d\Psi}{d\lambda}. \tag{12}$$

The solution to these equations with boundary conditions (9) is fully determined once we add the constitutive relation for P as a function of other fields; it is known analytically in the dilute limit $\varphi(n_0) \ll 1$, allowing the ideal gas approximation $Z(n) \approx 1$ and $P \approx MT$.

We do not recall the explicit form of the solution[39] for profiles M, V, and P (or T), which is long and not very informative. Still, using these expressions, all other quantities of interest may be derived. For instance, to estimate the energy of the Trinity bomb, Taylor computed the prefactor in the scaling law $R(t) = g(\gamma)(t\sqrt{E_0/\rho_0})^\delta$, that depends on the dimensionless parameter γ, using the conservation of energy,

$$\int_0^1 d\lambda\, M(\lambda)\left[\frac{V^2(\lambda)}{2} + \frac{P(\lambda)}{\gamma-1}\right] = E_0. \tag{13}$$

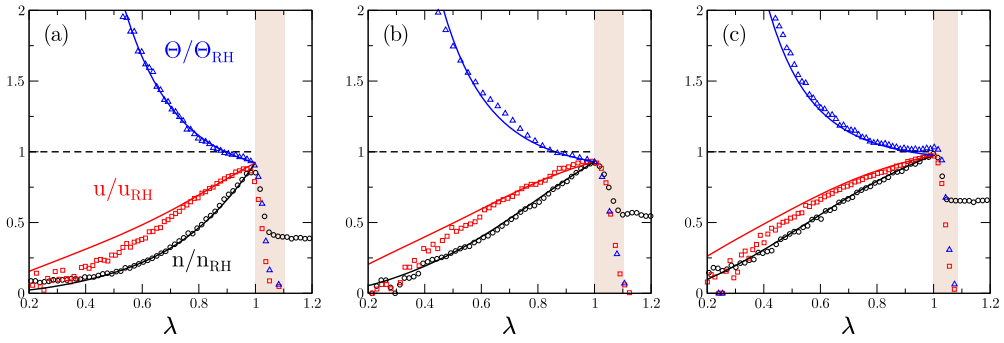

FIG. 2. Conservative blast at moderate densities. Hydrodynamic profiles rescaled by the theoretical boundary value (9) at $\lambda = 1$ the inner boundary of the shock front (shaded), for density n/n_{RH}, velocity u/u_{RH} and temperature Θ/Θ_{RH}. Initial volume fraction: (a) $\varphi_0 = 0.06$, (b) $\varphi_0 = 0.20$, (c) $\varphi_0 = 0.30$. Symbols are simulation results, and solid lines are hydrodynamic solutions of Eq. (11) where we imposed the empirical boundary values. The bulk equations seem to describe empirical profiles very accurately, especially in the outer part of the blast, as the theoretical temperature profile diverges at the center. However, there is a slight discrepancy in the boundary conditions (for instance, $n(1)/n_{RH} < 1$), reflecting the approximations involved in our computation of Rankine-Hugoniot conditions. Still, dimensionless profiles for all three fields converge to the same value at $\lambda = 1$, meaning that the scaling relations are correct. This is further illustrated in Fig. 4.

This prefactor $g(\gamma)$ was found to be close to unity, e.g., for tridimensional hard spheres $g(3/2) \approx 1.08$.

These profiles have been extensively tested experimentally,[3–5] and from hydrodynamic simulations.[40] However, to the best of our knowledge, they have hitherto not been confronted to microscopic simulations. Furthermore, we provide here the first approach accounting for higher densities via a more general constitutive relation: both the boundary conditions and the shape of the profiles are altered by the non-trivial equation of state $p = n\Theta Z(n)$. While not solvable analytically, they can still be integrated numerically with the choice for $Z(n)$ specified in Eq. (7). It thus remarkable to observe in Fig. 2 that TvNS-like solutions are confirmed by molecular dynamics for low-to-medium densities, except for the boundary values of the fields, whose Rankine-Hugoniot values seem overestimated. The slight discrepancy close to the center is expected as the TvNS approach predicts a temperature divergence, which is usually regularized by taking into account neglected transport terms such as heat conduction.[41]

Even more remarkable is the fact that this extended TvNS regime is limited. As the initial density n_0 is increased, the profiles observed in molecular dynamics simulations first follow, then diverge from those computed from Eqs. (11) and (7) by numerical integration. As we will show, this breakdown hinges on the fact that, in the classic solution, the flow velocity is everywhere subsonic *within the blast* (although supersonic compared to the outside medium) and any perturbation thus quickly diffuses and relaxes. By contrast, high density blasts may exhibit regions of supersonic flow, where the profiles cannot reach their asymptotic self-similar form as perturbations accumulate at the boundary.

To discuss this phenomenon, we must define the sound velocity as

$$c(r,t) = \sqrt{\gamma P(r,t)/n(r,t)}, \tag{14}$$

which appears naturally by considering the propagation of small compression waves around an homogeneous initial state and is thus expected to have local validity. Since we have assumed an adiabatic flow without heat waves, and there is no transverse velocity field, any perturbation should be in the form of acoustic waves. Thus, the maximal and minimal velocity of an energy-carrying perturbation are typically $u(r,t) + c(r,t)$ and $u(r,t) - c(r,t)$, depending on whether it is carried by the flow or going against it. By contrast, the phase velocity of the blast is $\lambda\dot{R}$, the geometric speed of a point at a fixed value of $\lambda = r/R(t)$. If this phase velocity exceeds the maximal, some regions within the blast become isolated from others. This is usually checked by representing profiles $c(r,t)$ and $u(r,t)$ on the parametric graph $c(u)$ (see Figure 3) where the *sonic line* is defined by

$$u(r,t) + c(r,t) = \lambda\dot{R}(t). \tag{15}$$

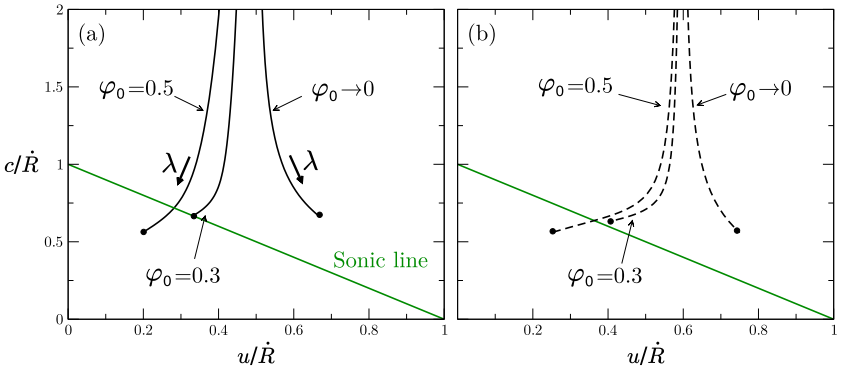

FIG. 3. Phase portrait $c(u)$ for a conservative blast with finite density: the three curves are parametric representation of the sound velocity as a function of the flow velocity, as obtained by numerical integration of Eq. (11). The dimensionless profiles depend only on $\lambda \in [0,1]$, which is increasing in the direction of the bold arrows. Dots correspond to the location of the front $\lambda = 1$. We represent solutions (a) in dimension 2 and (b) in dimension 3 for some values of the initial volume fraction φ_0. The straight line locates the sonic line $u + c = \lambda\dot{R}$. The critical value of φ_0 for which the sonic line is reached by the profiles depends on the spatial dimension but stays close to 0.3.

If the profile $c(u)$ stays above this line, perturbations are always faster than the phase velocity; this is the case of the dilute TvNS solution, but not of profiles found for high densities. Any singularity in the flow (that does not involve a shock and thus some compression) must lie on the sonic line — or any other characteristic line corresponding to another relevant physical speed being equal to the phase velocity,[42] i.e., $u = \lambda\dot{R}$ and $u - c = \lambda\dot{R}$. We find indeed that this point separates the region where the dense TvNS solution describes numerical profiles correctly from that where it fails. This illustrated in Fig. 4, and in particular evidenced by the temperature profile (upper curve), which becomes non-monotonous when plagued with supersonic effects. On the other hand, the density profile is still in good agreement with its TvNS counterpart.

D. Dissipative blast

The previous detour through conservative blasts demonstrated the importance of the equation of state. In the case of a dissipative blast, due to the accretion into a shell, asymptotic densities

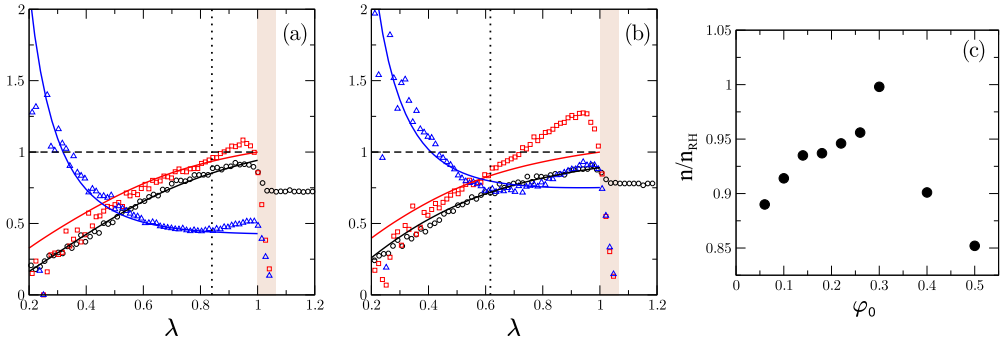

FIG. 4. Conservative blast at high densities. Density, velocity, and temperature profiles (see details in Fig. 2) in two cases where phase velocity is supersonic immediately behind the shock: (a) $\varphi_0 = 0.40$ and (b) $\varphi_0 = 0.50$. By contrast with the case of entirely subsonic solutions $\varphi_0 \le 0.30$, the profiles disagree with the asymptotic hydrodynamic solution (solid lines) and do not converge toward boundary values that are compatible with each other. The dotted vertical line marks the abscissa where theoretical profiles cross the sonic line $u(r,t) + c(r,t) = \lambda\dot{R}(t)$, which does indeed appear to be the point where the velocity and temperature profiles deviate from model predictions, with temperature becoming non-monotonic. (c) Ratio between the measured and theoretical compressions at the boundary $n(1)/n_{RH}$ as a function of φ_0, with the surprising effect that the best agreement is found for a large value of $\varphi_0 \approx 0.3$. This may be understood as resulting from the fact that the compression through the shock is smaller for larger initial volume fractions, thus limiting the importance of higher order effects.

within are necessarily very high, and thus the flow must be described as dense fluid. To the best of our knowledge, the single previous attempt at elucidating the full structure of a dissipative blast[32] was committed to an ideal gas description that could not capture the phenomena we observe in simulations, including the instability discussed in Sec. IV.

Instead, we will show that the dissipative coarse-grained Equations (2) admit a solution that closely matches numerical measurements. This solution exhibits an anisotropic pressure tensor acting only along the radial direction $\mathbf{e}_r$ and of the form

$$\mathbf{p} = n\,\Theta\,Z(n)\,\mathbf{e}_r \otimes \mathbf{e}_r \tag{16}$$

with $Z(n)$ an adequate choice of constitutive law.

The boundary conditions on these three profiles are set by the fixed width sector, including the front (or mixing layer) where temperature is created, and the cooling region where it is dissipated. This sector is not self-similar, but we can make another simplifying assumption to make the equations tractable. If the gradients mostly occur along the normal to the shock boundary, the flow in that region can be approximated as one-dimensional; this approximation improves as this layer's fixed width becomes small compared to its increasing curvature radius. This allows us to simplify Eqs. (2) by considering them only along the radial direction, and integrate them between $r = R(t) - x$ and $R(t)$ giving

$$n(x) = n_{\text{rest}} M(x), \quad u = \dot{R}\left[1 - \frac{1}{M}\right], \quad p = n_{\text{rest}} \dot{R}\, u. \tag{17}$$

This flux-difference form[30] is similar to the one usually employed for the shock front itself, and we recover the Rankine-Hugoniot conditions of Sec. II B (see also the supplementary material) by letting $x \to 0$. All three fields are parameterized by compression $M(x)$ solving the following equation (which may be integrated numerically for any choice of $Z(n)$):

$$(M-1)\left[\frac{d}{2}Z^{-1} + 1\right] = \frac{M^2}{2} - \omega_0(1-\alpha^2)\int_{0^-}^{x} dx' \left(\frac{d(M-1)}{2Z}\right)^{3/2}, \tag{18}$$

where the latter term stems from collisional dissipation. Higher-order transport terms neglected in Eqs. (2) may in fact intervene in this intermediary region, which has no growing typical length scale; the present simplified analysis proves sufficient for our purposes though.

The fixed-width cooling layer is pushed outward by the expanding cold region, where the absence of temperature allows self-similarity to take hold again, by neglecting the main dissipation term in the hydrodynamic equations. We can look for profiles in analogy with Eq. (10), except for the temperature field: it could previously be used interchangeably with the pressure field, via the constitutive relation, but it is now vanishingly small while $Z(n)$ diverges due to steric effects. In fact, a simplified analytic solution can be obtained assuming the fluid to be incompressible and at random close packing density $n_{\text{rcp}} = n_{\text{rest}} M_{\text{rcp}}$, a fair approximation corresponding to a volume fraction $\varphi_{\text{rcp}} \approx 0.84$ for $d = 2$ or 0.64 for $d = 3$. The profiles for velocity and pressure are then

$$\begin{aligned} V(\lambda) &= \delta\left(1 - M_{\text{rcp}}^{-1}\right)\lambda^{-d}, \\ P(\lambda) &= \delta^2\,\lambda^2\left(1 - M_{\text{rcp}}^{-1}\right)\left(M_{\text{rcp}}(\lambda^d - 1) + 1\right). \end{aligned} \tag{19}$$

These two solutions can be joined in a piecewise fashion by applying the criterion that the cooling layer stops as soon as the density reaches its random close packing value $n = n_{\text{rcp}}$, at $r_c = R(t)\lambda_c(t)$ (with $\lambda_c(t) \to 1$ since the cooling layer is of fixed width while $R(t)$ increases). The inner boundary of the cold region, separating it from the empty core, is also rigorously defined: it is given by λ_i such that

$$\dot{R}\lambda_i = u(\lambda_i), \tag{20}$$

meaning that the flow velocity is equal to the phase velocity: this necessarily coincides with pressure vanishing, and with any boundary with an empty region of space, as it means that the velocity of the wave at that point is exactly that of the last particles, i.e., the boundary is defined by these particles moving out and emptying the space behind them. Assuming that the cooling layer is of

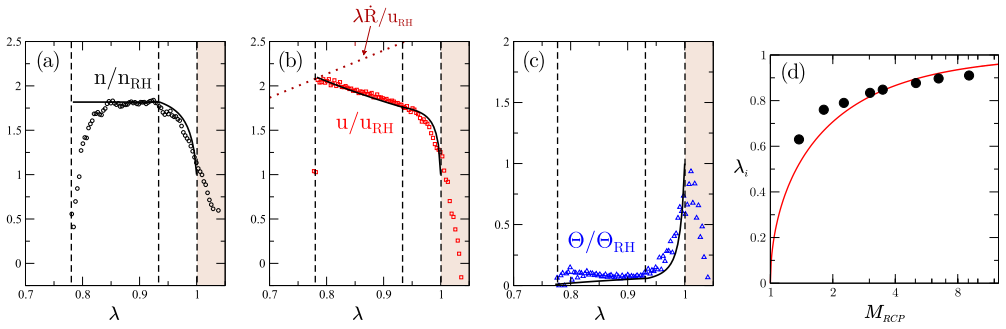

FIG. 5. Dissipative blast in spatial dimension $d = 2$. Hydrodynamic profiles rescaled by their Rankine-Hugoniot value defined in Sec. II B. (a) $n(\lambda)/n_{RH}$, (b) $u(\lambda)/u_{RH}$, and (c) $\Theta(\lambda)/\Theta_{RH}$ with $\lambda = r/R(t)$. Thick lines are analytic solutions, symbols are measurements from molecular dynamics simulations. These figures display the spectacular divergence of the solution from the elastic case for any value $\alpha < 1$ (here $\alpha = 0.8$), with the bulk of the blast dividing into multiple regions. Vertical lines represent the inner boundaries of these regions: the front (shaded, the mixing region where some particles are still at rest) which lies above the boundary $\lambda = 1$ where fields reach their Rankine-Hugoniot value and temperature is maximal; the cooling region between $\lambda = 1$ and $\lambda = \lambda_c$ defined as the point where density reaches its random close packing value in the calculated profiles, and the cold gas down to $\lambda = \lambda_i$ where pressure vanishes and the flow velocity equals the phase velocity. (d) Approximation (21) for λ_i as a function of the compression ratio $M_{RCP} = n_{RCP}/n_0$ (solid line) and late-time measurements in simulations (dots). The approximation ignores the width of the cooling layer, which is asymptotically negligible. Even so, we find a reasonable estimate $1 - \lambda_i \approx 0.15$ for the width of the cold region in the profiles shown here, with $M_{RCP} = \approx 3.5$.

negligible width (as is asymptotically true), we then find

$$\lambda_i \approx \left(1 - M_{RCP}^{-1}\right)^{1/d}. \tag{21}$$

Since all other boundary conditions are rigorously computed and have well-defined locations, there is no fitting parameter in the model. This piecewise solution is seen in Fig. 5 to be in excellent agreement with the profiles measured in molecular dynamics simulations, including the locations λ_c and λ_i of the boundaries between regions.

The boundary λ_i is also seen to correspond to the maximal flow velocity in the system, which fits with the intuition that the blast wave moves inertially and is being pushed outward by the innermost particles. The rest are slowed down by the dissipative collisions and accrete onto the incoming "snowplow." It therefore appears that in the present inelastic case, radial coherent motion decouples from that taking place in the perpendicular direction (incoherent motion). This is in contrast with the elastic situation, where a single scaling in time does exist for both coherent and incoherent motions. This decoupling lays the ground for the possibility of new scaling behaviors, as compared to standard conservative TvNS phenomenology.

III. SCALING LAWS

A. Conservation of momentum

Previous works[22] have already confirmed that Oort's proposed asymptotic regime for dissipative blasts, the momentum-conserving snowplow (MCS)[15] based on the global conservation of *radial* momentum, is observed in simulations of inelastic hard spheres, as we show in Fig. 6. However, no rigorous justification for that conservation law has been proposed, and evidence in experiments on granular flows is unclear.[20,21] Using our hydrodynamic model, we can now investigate the conditions under which the conservation of radial momentum can arise in a granular flow, while it is absent from most types of blasts, including the classical TvNS solution.

Let us first recall Equation (2b) for the local conservation of momentum and write it in the case of isotropic pressure $\mathbf{p} = p\mathbf{I}$ as in the TvNS solution,

$$\partial_t(nu) + \mathrm{div}\left(nu^2\right) + \partial_r p = 0. \tag{22}$$

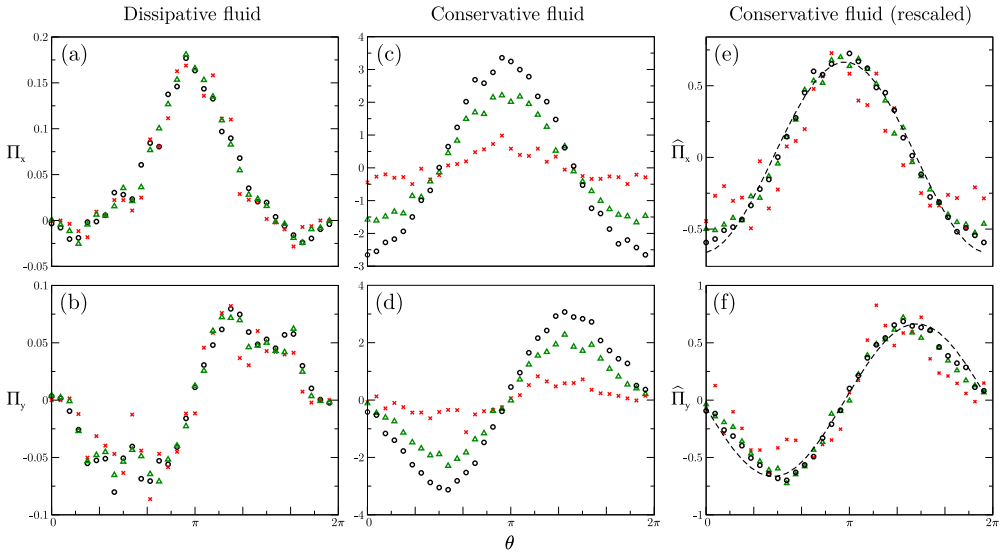

FIG. 6. Conservation of total momentum per angular sector $\Pi(\theta)$ in a two-dimensional molecular dynamics simulation. Panels (a) and (b) demonstrate the conservation of the x- and y-component of $\Pi(\theta)$ over time in the dissipative blast ($\alpha = 0.2$). Panels (c)-(f) focus on the energy-conserving blast: (c) and (d) display the increasing radial momentum $\Pi(\theta)$, while (e) and (f) show it rescaled by its theoretical time dependence, $\widehat{\Pi}(\theta) = \Pi(\theta)/t^{d/(d+2)}$. Symbols correspond to numerical measurements at successive times $t = 1, 10, 20$ (crosses, triangles, and circles, respectively), while the dashes give the expected value under the assumption of perfect isotropy, $\widehat{\Pi}_x \propto -\cos\theta$ and $\Pi_y \propto -\sin\theta$.

Integrating over an angular sector of width $d\theta$ around angle θ (or likewise with solid angles if $d > 2$), we find

$$\partial_t \Pi(\theta,t) = \partial_t \int_0^\infty nu\, r^{d-1} dr = \left[nu^2 + p\right]_0^\infty - (d-1)\int_0^\infty p r^{d-2} dr, \tag{23}$$

where we dropped the (r,θ,t) dependency. Velocity and pressure are both zero in the gas at rest, and density is vanishingly small at the center of the blast (even in the TvNS solution), so that

$$\partial_t \Pi(\theta,t) = p(0,\theta,t) - (d-1)\int_0^\infty p(r,\theta,t) r^{d-2} dr. \tag{24}$$

This formula adequately describes a range of possible phenomena. If the central pressure dominates the expansion, the total momentum per angular sector $\Pi(\theta,t)$ increases with time, as observed for the conservative blast in the central panel of Fig. 6. On the other hand, in a hollow blast solution with no central pressure $p(0,\theta,t) = 0$, we find that $\Pi(\theta,t)$ decreases with time, as observed in certain conservative blasts which are forced to adopt a hollow structure[43]— either for gases with $\gamma \gtrsim 1$, or when the density of the external medium decreases strongly with radial distance r. Orthoradial momentum transfers occur within the shell itself which cause radial momentum to decrease, and thus slow down the expansion, leading to scaling exponents $\delta < 1/(d+1)$.

The exact conservation of radial momentum that is at the core of the MCS solution is only found if orthoradial transfers cannot take place. In extremely dilute fluids such as found in astrophysics, the usual argument is that the shell will be so thin that we may neglect any transfers happening within. However, the granular blast has a non-negligible thickness and still exhibits the scaling regime. Orthoradial transfers vanish identically if the pressure is not isotropic but purely radial, i.e., $\mathbf{p} = p\mathbf{e}_r \otimes \mathbf{e}_r$, in which case the total momentum per angular sector can change only due to central pressure,

$$\partial_t \Pi(\theta,t) = p(0,\theta,t), \tag{25}$$

and is therefore conserved in a hollow blast. A strong anisotropy of pressure is in fact commonly observed in granular flows[44] and it is expected to appear here due to the existence of a privileged direction. In the supplementary material, we discuss the consequences of relaxing this assumption.

The momentum conservation principle that controls the similarity regime of the dissipative blast can thus only be understood in the light of microscopic insight, whereas continuum approaches usually posit isotropic pressure by default and face a contradiction.

B. Intermediate regimes

We may then consider the succession of intermediate regimes that govern the evolution of the system before the MCS phase. A scaling regime is characterized by a value of exponent δ in the scaling law $R(t) \sim t^{\delta}$, from which all other scaling exponents can easily be derived by dimensional analysis. As explained above, both pressure at the center and orthoradial momentum transfers must vanish to enter the radial momentum-conserving regime.

However, let us consider the possibility that orthoradial exchanges in the shell vanish before the central pressure. The latter may be caused by a small number of comparatively energetic particles that populate the hollow core, and have yet to accrete into the shell. Then, the right-hand term is non-zero in Eq. (25). Further assuming that the very dilute gas in the cavity obeys the law of adiabatic expansion (density is low enough for dissipation and other effects to be negligible), and given that the volume of the cavity is proportional to R^d, we have $P(R^d)^{\gamma} = \text{constant}$. An intermediate regime, known as the Pressure-Driven Snowplow (PDS),[45] can therefore arise with exponent $\delta = 2/(d\gamma + 2) \geq 1/(d+1)$. It is self-similar of the second kind, varying with the adiabatic index γ which is a nondimensional microscopic parameter of the dynamics.

While it relies on strong assumptions, this derivation has found empirical validation[6] and Fig. 7 gives the first evidence from molecular dynamics simulations for this succession of regimes in a granular gas. Since our simulated system is comprised of hard spheres, with the standard adiabatic index $\gamma = 1 + 2/d$, the exponent for the PDS regime is $\delta = 2/(d+4)$. As this causes the PDS and MCS exponents to be accidentally identical in spatial dimension $d = 2$, the figure instead presents results from simulations in dimension $d = 3$ where $\delta = 2/(d+4) = 2/7$ for the PDS regime and $1/(d+1) = 1/4$ for the MCS regime.

C. Comparison with experiments

Experiments on the granular blast[20,21] have not conclusively revealed the existence of the MCS regime, or even any of the intermediate regimes discussed above; instead, authors propose a logarithmic growth, supported by analytical arguments. We now discuss how the previous analysis may provide hints to understand this apparent discrepancy.

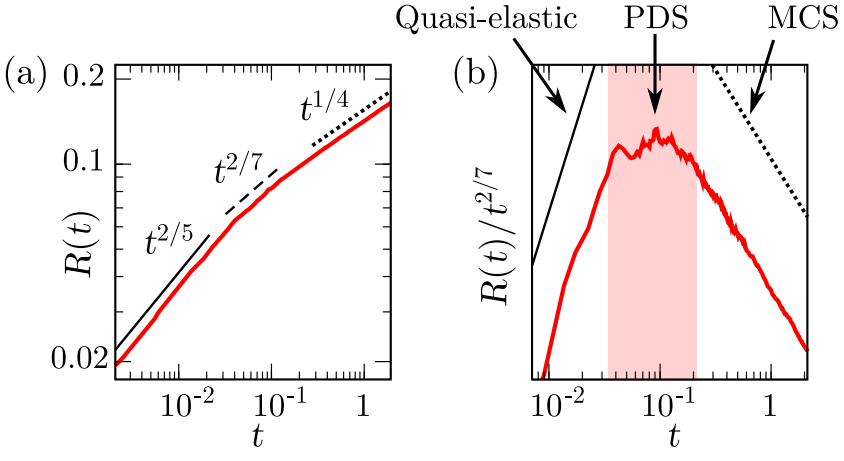

FIG. 7. Scaling of the radius $R(t)$ in a three dimensional simulation ($d = 3$). There are three successive regimes: quasi-elastic $t^{2/(d+2)}$ (solid line) before dissipation becomes significant, then Pressure-Driven Snowplow (PDS, dashes) $t^{2/(d\gamma+2)}$, and Momentum-Conserving Snowplow (MCS, dots) $t^{1/(d+1)}$. (a) Raw data. (b) Data rescaled by the PDS law, to evidence that regime over one decade (shaded region).

Let us first recall the experimental setting. Small beads are flowing down a slope, a massive ball is dropped from above, hits the slope and imparts energy to surrounding beads, and finally rebounds off, exiting the system. The expanding crown of beads excited by the collisions is then observed in the referential of the flow, moving along the slope. A crucial aspect of these experiments is that the blast starts with a peculiar initial condition: a hollow central region is created as beads are displaced from the contact area of the ball with the slope.

Following the discussion in Sec. III A, it is thus possible that the expansion of the blast first obeys a power-law with exponent inferior to $1/(d+1)$: before dissipation causes them to vanish, orthoradial momentum transfers may yet persist inside the expanding shell of beads, while central pressure has been eliminated since the blast is created with an inner cavity. As explained before, this causes radial momentum to decrease and leads to slower expansion than in the MCS regime. Another possibility is that the similarity regime is simply never observed, as the external medium has finite temperature, and strong shock conditions do not hold for long, despite the fact that the shock is created with high Mach number[21] $M \approx 10$.

Finally, the logarithmic regime proposed in the analysis of the experiment[20] deserves further discussion: it is indeed possible as a transient regime before similarity takes hold. It is not fully self-similar, but driven by energy dissipation in the travelling wave-like cooling layer that immediately follows the shock front (see Sec. II D), making no assumption on the form of hydrodynamic fields in the innermost regions, except that they exert negligible outward pressure on the cooling layer. As discussed in a previous work,[46] a very similar phenomenon is seen in a one-dimensional system, where the shock front and cooling region at first reduce to a single leading particle, which decelerates geometrically with collisions and thus propagates logarithmically. It is only when following particles catch up and push it from behind that the wave evolves toward the eventual scaling regime. In higher dimensions, this regime typically requires the suppression of central pressure to be observed, as it holds only as long as the core cannot push outward on the shell (consistently with an initial hollow core, transiently filling up with particles and energy that drop out of the shell), and it is thus a good candidate to explain experimental findings.

IV. CORRUGATION INSTABILITY

Numerical studies of the granular blast[22,47,48] have remarked that the shape of the shock boundary is preserved: contrary to the conservative case where central pressure pushes particles outward isotropically, the dissipative blast region does not tend to evolve toward central symmetry with a clear circular (or spherical) boundary. Instead, it retains any anisotropy it had at the start of the self-similar regime, as a result of random collisions during the transient phase, see Fig. 1. Symmetry can be imposed to this shape by distributing the initial excitation over a disk or sphere, or by using particles with low enough inelasticity that the blast first becomes isotropic in a quasi-elastic phase before evolving toward the dissipative asymptotics.

This peculiar property of marginal stability should not be confused with the previously unobserved phenomenon that we discuss here: whether anisotropic or not, the basic self-similar shape of the boundary is later overtaken by a corrugation instability (see Fig. 8) that causes the appearance of ripples, themselves growing self-similarly. This can be revealed by a linear stability analysis which we detail in Appendix 3 of the supplementary material. We focus on the two-dimensional case with central symmetry, as it is most relevant to granular experiments.[49] For each field Ψ, we thus assume a relative perturbation which depends on time and angle θ as follows:

$$\Psi(\mathbf{r},t) = \Psi_0(\lambda)(1 + \delta\Psi(\lambda)\cos(k\theta)t^s), \tag{26}$$

with Ψ_0 the scaling solution derived above in the cold region. Likewise, $R(t) = R_0(t)(1 + \delta R(\lambda)\cos(k\theta)t^s)$, and we consider the conditions under which exponent s is positive, leading to a loss of stability of the reference solution.

Profiles for the eigenmodes of the perturbation can be obtained by integrating the linearized equations given in the supplementary material. These contain two parameters: k the wave number, and s the growth exponent, which appears both in the bulk equations and in the boundary conditions. For any value of k, there is only one value of $s(k)$ that allows the profiles to satisfy both

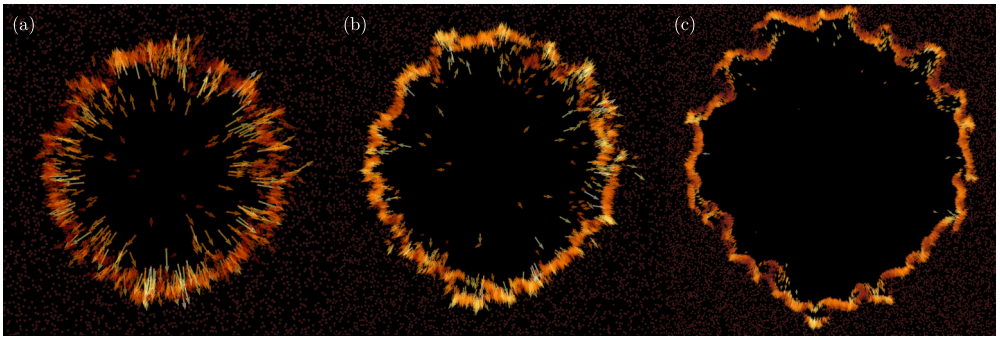

FIG. 8. Blast particles and velocities for $\alpha = 0.3$ and $\varphi_0 = 0.1$ at times (a) $t = 8$, (b) $t = 20$, (c) $t = 40$. All distances are rescaled by $R(t) \sim t^{\delta}$, and the initial excitation was distributed over a circular region to clearly observe the growth of the instability around an isotropic self-similar solution (if the dissipative blast is given an initial anisotropy, the asymmetric shape it acquires in the early expansion tends to be preserved by the subsequent inertial growth).

outer and inner boundary conditions; however, analytical integration is not possible, therefore we must use a shooting algorithm: for every sampled k, we test values of s by using them to integrate the profiles numerically from the outer boundary inward, and we select $s(k)$ which minimizes the distance between the measured profiles at the inner boundary and their theoretical value. This method, previously proposed[50] to study instabilities in a different class of blasts, allows to extend linear stability analysis in the case of reference solutions which are neither uniform nor stationary, and thus do not easily allow for analytical treatment. This approach is however cumbersome and encounters numerous convergence problems, as the boundaries are singular points and perturbation profiles are often found to diverge in that limit (see discussion in the supplementary material).

Nevertheless, Fig. 9 demonstrates that this method produces conclusive results. The dispersion relation $s(k)$ is found for each of the three eigenmodes with wave number k in the set of three equations given in the supplementary material. Two of these modes are oscillatory in nature and convergent ($\Re(s) < 0$, $\Im(s) \neq 0$) while the last mode reveals a non-oscillating instability: $s(k)$ is real and $s(k) > 0$ for $k > k_c$.

While the shooting algorithm has increasing convergence problems for high k, which do not allow to sample arbitrarily high values of the wave number, the obtained dispersion relation for the leading mode appears to have a maximum at $s \approx 0.3$, or perhaps even a plateau that might extend indefinitely. The ordinate of this plateau does not depend on any of the parameters of the model, e.g., α or φ_0, as they are entirely absent from the stability analysis above. Crucially, this value

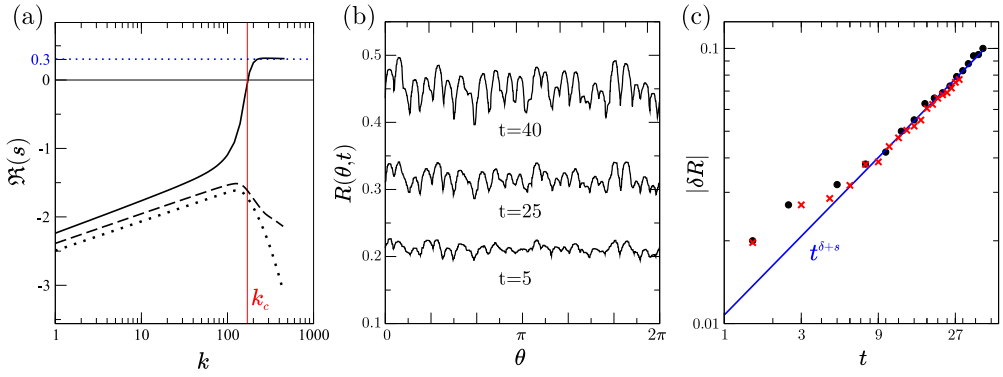

FIG. 9. The corrugation instability in a dissipative blast. (a) Real part of the dispersion relation $\Re s(k)$ for all three modes. The unstable mode crosses the origin at $k_c \approx 160$ and has a plateau at $s \approx 0.3$. It is also strictly real, while the two vanishing modes have constant imaginary components (not shown). (b) Plot of the corrugation growth $R(\theta, t)$ for different times. (c) Numerical verification of the exponent $s \simeq 0.3$ for values of α equal to 0.3 (circles) and 0.8 (crosses).

$s \approx 0.3$ is precisely the measured exponent for the relative growth of the corrugation amplitude in simulations, which is also independent of these parameters (see Fig. 9).

Let us now discuss the peculiarities of this phenomenon, and in what it differs from previously reported classes of instabilities. First, the growth of the corrugation is itself self-similar even for short times. This distinguishes it from the best-known Rayleigh-Taylor type, characterized by an initial exponential growth, in which self-similarity can occur only for late times and under certain specific conditions.[51] The power law structure suggests that the instability takes place in the cold gas region, and, as our analysis shows, hinges on the layered structure of the solution. For that reason, the details of the microscopic parameters like the value of inelasticity or the initial density of the gas do not affect the behavior of the corrugation, giving a universal fingerprint to this phenomenon. The vanishing pressure at the center is a distinctive characteristic and a necessary condition for the instability to take place. If a finite pressure is imposed at the boundary, as in a piston-like setup, the instability completely changes in nature, losing its self-similar structure and showing the presence of convective rolls.[52] On the contrary, the vanishing pressure ensures the conservation of momentum per angular sector, which is maintained even after the corrugation instability appears. This leads to the following interpretation: density fluctuations in the gas produce a slowing down of some points of the front and a consequent discrepancy in the propagation velocity of neighboring regions, producing the effect of slosh dynamics between the cold gas and the particles at rest. This mechanism is quite different from the one proposed in the blast waves propagating in uniform gases: in that case, a net pressure wave along the front of the blast is observed, producing oscillations in the hydrodynamics fields. This latter description is more consistent with a dispersion relation with an imaginary contribution, instead of the pure real value of the exponent s observed in our case.

V. CONCLUSION

We have established a bridge between the coarse-grained view of strong shocks and a microscopic level of description. While we have put the emphasis on dissipative media, our analysis led us to revisit the more traditional problem of Taylor-von Neumann-Sedov blasts in conservative fluids. It appears that in both cases, the dynamics of the blast exhibits self-similarity of the first kind, therefore grounded in conservation laws rather than in microscopic details. Yet, the corresponding scaling laws are drastically affected by energy dissipation, a key feature being that coherent and incoherent motion decouple in the dissipative case, while they are always coupled, and therefore endowed with similar scaling behavior, when energy is conserved. We have discussed the microscopic origin of momentum conservation in different angular sectors of the shocks, which characterizes the inelastic dynamics and from which scaling exponents readily follow, stressing that this conservation law breaks down for elastic situations, although binary collisions conserve momentum in all cases. Furthermore, depending on initial conditions, intermediate nontrivial scaling regimes can be evidenced, see e.g., Figure 7.

Beyond scaling, we have provided an accurate hydrodynamic description for the coupled density, pressure, and kinetic temperature fields. We have shown that the simple Taylor-von Neumann-Sedov solution can be adapted for dense conservative fluids, and successfully describes a flow simulated at the kinetic level, but breaks down at high densities with the development of supersonic regions within the blast. On the other hand, shocks in dissipative fluids exhibit a rather complex structure, with an asymptotic hollow core that has no counterpart in conservative blasts. Its multi-layered structure is an important ingredient in a successful analytical description, together with the inertial nature of its dynamics. Finally, we have shown that the self-similar solution brought to bear is plagued by a corrugation instability, which exhibits some peculiar features. Indeed, the structure of this instability is itself similar and does not depend on the microscopic parameter of the system nor on the specific geometry studied (similar behaviors are found in planar and three-dimensional geometries[53]). Essential for the occurrence of the corrugation are the development of a zero-temperature layer of accreted particles moving coherently, and the vanishing pressure in the innermost region of the blast.

SUPPLEMENTARY MATERIAL

See the online supplementary material for a review of classic results and the state of the art, details on numerical and analytical methods including boundary conditions and the linear stability analysis, and additional discussion of the ansatz of anisotropic pressure.

ACKNOWLEDGMENTS

We thank J. F. Boudet, A. Vilquin, H. Kellay, and P. Krapivsky for discussions.

[1] G. Taylor, "The formation of a blast wave by a very intense explosion. I. Theoretical discussion," Proc. R. Soc. London, Ser. A **201**, 159–174 (1950).
[2] G. Taylor, "The formation of a blast wave by a very intense explosion. II. The atomic explosion of 1945," Proc. R. Soc. London, Ser. A **201**, 175–186 (1950).
[3] J. M. Dewey, "The air velocity in blast waves from t.n.t. explosions," Proc. R. Soc. London, Ser. A **279**, 366–385 (1964).
[4] A. Edens, T. Ditmire, J. Hansen, M. Edwards, R. Adams, P. Rambo, L. Ruggles, I. Smith, and J. Porter, "Study of high mach number laser driven blast waves," Phys. Plasmas **11**, 4968 (2004).
[5] A. Moore, D. Symes, and R. Smith, "Tailored blast wave formation: Developing experiments pertinent to laboratory astrophysics," Phys. Plasmas **12**, 052707 (2005).
[6] D. F. Cioffi, C. F. McKee, and E. Bertschinger, "Dynamics of radiative supernova remnants," Astrophys. J. **334**, 252 (1988).
[7] J. Ostriker and C. McKee, "Astrophysical blastwaves," Rev. Mod. Phys. **60**, 1–68 (1988).
[8] G. I. Barenblatt, *Scaling, Self-Similarity, and Intermediate Asymptotics: Dimensional Analysis and Intermediate Asymptotics* (Cambridge University Press, 1996), Vol. 14.
[9] A. Vogel, S. Busch, and U. Parlitz, "Shock wave emission and cavitation bubble generation by picosecond and nanosecond optical breakdown in water," J. Acoust. Soc. Am. **100**, 148–165 (1996).
[10] R. H. Cole, *Underwater Explosions* (Dover Publications, 1965).
[11] V. K. Kedrinskiy, *Hydrodynamics of Explosion: Experiments and Models* (Springer Science & Business Media, 2006).
[12] C. Cavet, H. C. Nguyen, C. Michaut, E. Falize, S. Bouquet, and L. Menza, "Theoretical and numerical studies of the Vishniac instability in supernova remnants," Astrophys. Space Sci. **322**, 91–95 (2008).
[13] R. Sari, N. Bode, A. Yalinewich, and A. MacFadyen, "Slightly two- or three-dimensional self-similar solutions," Phys. Fluids **24**, 087102 (2012).
[14] T. Antal, P. Krapivsky, and S. Redner, "Exciting hard spheres," Phys. Rev. E **78**, 030301 (2008).
[15] J. Oort, "Problems of cosmical aerodynamics," in Central Air Document Office, Dayton, 1951.
[16] J. Ostriker and J. Silk, "Dust cooling of hot gas," Astrophys. J. **184**, L113 (1973).
[17] M. Colangeli, *From Kinetic Models to Hydrodynamics: Some Novel Results* (Springer, 2013).
[18] N. V. Brilliantov and T. Pöschel, *Kinetic Theory of Granular Gases* (Oxford Graduate Texts, 2004).
[19] A. Puglisi, *Transport and Fluctuations in Granular Fluids: From Boltzmann Equation to Hydrodynamics, Diffusion and Motor Effects* (Springer, 2014).
[20] J. Boudet, J. Cassagne, and H. Kellay, "Blast shocks in quasi-two-dimensional supersonic granular flows," Phys. Rev. Lett. **103**, 224501 (2009).
[21] J.-F. Boudet and H. Kellay, "Unstable blast shocks in dilute granular flows," Phys. Rev. E **87**, 052202 (2013).
[22] Z. Jabeen, R. Rajesh, and P. Ray, "Universal scaling dynamics in a perturbed granular gas," Europhys. Lett. **89**, 34001 (2010).
[23] M. Barbier, D. Villamaina, and E. Trizac, "Blast dynamics in a dissipative gas," Phys. Rev. Lett. **115**, 214301 (2015).
[24] J. Brey, J. Dufty, C. Kim, and A. Santos, "Hydrodynamics for granular flow at low density," Phys. Rev. E **58**, 4638 (1998).
[25] J. Jenkins and S. Savage, "A theory for the rapid flow of identical, smooth, nearly elastic, spherical particles," J. Fluid Mech. **130**, 187–202 (1983).
[26] V. Garzó and J. Dufty, "Dense fluid transport for inelastic hard spheres," Phys. Rev. E **59**, 5895 (1999).
[27] S. Chapman and T. Cowling, *The Mathematical Theory of Non-Uniform Gases: An Account of the Kinetic Theory of Viscosity, Thermal Conduction, and Diffusion in Gases* (Cambridge University Press, 1991).
[28] P. Reinicke and J. Meyer-ter Vehn, "The point explosion with heat conduction," Phys. Fluids A **3**, 1807 (1991).
[29] L. Landau and E. Lifshitz, *A Course in Theoretical Physics-Fluid Mechanics* (Pergamon Press Ltd., 1987).
[30] A. Goldshtein, M. Shapiro, and C. Gutfinger, "Mechanics of collisional motion of granular materials. III. Self-similar shock wave propagation," J. Fluid Mech. **316**, 29 (1996).
[31] T. Pöschel and N. Brilliantov, *Granular Gas Dynamics* (Springer Verlag, 2003).
[32] E. Bertschinger, "On the structure and stability of radiative shock waves," Astrophys. J. **304**, 154 (1986).
[33] A. Santos, J. Montanero, J. Dufty, and J. Brey, "Kinetic model for the hard-sphere fluid and solid," Phys. Rev. E **57**, 1644–1660 (1998).
[34] M. Baus and J. Colot, "Thermodynamics and structure of a fluid of hard rods, disks, spheres, or hyperspheres from rescaled virial expansions," Phys. Rev. A **36**, 3912 (1987).
[35] D. Henderson, "A simple equation of state for hard discs," Mol. Phys. **30**, 971–972 (1975).
[36] A. Santos, M. De Haro, and S. Yuste, "An accurate and simple equation of state for hard disks," J. Chem. Phys. **103**, 4622 (1995).
[37] A. Goldshtein and M. Shapiro, "Mechanics of collisional motion of granular materials. I. General hydrodynamic equations," J. Fluid Mech. **282**, 75 (2006).
[38] I. Pagonabarraga, E. Trizac, T. Van Noije, and M. Ernst, "Randomly driven granular fluids: Collisional statistics and short scale structure," Phys. Rev. E **65**, 011303 (2001).

[39] L. Sedov, *Similarity and Dimensional Analysis in Mechanics* (Academic Press, New York, 1959).
[40] J. R. Kamm, "Evaluation of the Sedov-von Neumann-Taylor blast wave solution," Technical Representative, Los Alamos National Laboratory Report No. LA-UR-00-6055, 2000.
[41] A. Abdel-Raouf and W. Gretler, "Quasi-similar solutions for blast waves with internal heat transfer effects," Fluid Dyn. Res. **8**, 273–285 (1991).
[42] D. Kushnir and E. Waxman, "Closing the gap in the solutions of the strong explosion problem: An expansion of the family of second-type self-similar solutions," Astrophys. J. **723**, 10 (2010).
[43] J. Sanz, S. Bouquet, and M. Murakami, "Self-consistent stability analysis of spherical shocks," Astrophys. Space Sci. **336**, 195–200 (2011).
[44] A. Barrat and E. Trizac, "Molecular dynamics simulations of vibrated granular gases," Phys. Rev. E **66**, 051303 (2002).
[45] C. McKee and J. Ostriker, "A theory of the interstellar medium-three components regulated by supernova explosions in an inhomogeneous substrate," Astrophys. J. **218**, 148–169 (1977).
[46] M. Barbier, "Kinetics of blast waves in one-dimensional conservative and dissipative gases," J. Stat. Mech.: Theory Exp. **2015**, P11019.
[47] S. Pathak, Z. Jabeen, P. Ray, and R. Rajesh, "Shock propagation in granular flow subjected to an external impact," Phys. Rev. E **85**, 061301 (2012).
[48] S. N. Pathak, Z. Jabeen, R. Rajesh, P. Ray, R. Mittal, A. Chauhan, and R. Mukhopadhyay, "Shock propagation in a visco-elastic granular gas," AIP Conf. Proc. **1447**, 193 (2012).
[49] J. Boudet, Y. Amarouchene, and H. Kellay, "Shock front width and structure in supersonic granular flows," Phys. Rev. Lett. **101**, 254503 (2008).
[50] D. Kushnir, E. Waxman, and D. Shvarts, "The stability of decelerating shocks revisited," Astrophys. J. **634**, 407–418 (2005).
[51] A. W. Cook, W. Cabot, and P. L. Miller, "The mixing transition in Rayleigh–Taylor instability," J. Fluid Mech. **511**, 333–362 (2004).
[52] N. Sirmas and M. I. Radulescu, "Evolution and stability of shock waves in dissipative gases characterized by activated inelastic collisions," Phys. Rev. E **91**, 023003 (2015).
[53] M. Barbier, "De limpermanence des formes dans les fluides granulaires," Ph.D. thesis Doctoral dissertation, Université Paris-Sud, 2012.